TiO$_2$ nanotubes with different spacing, Fe$_2$O$_3$ decoration and their evaluation for Li-ion battery application

Selda Ozkan[1†], Gihoon Cha[1†], Anca Mazare[1] and Patrik Schmuki[1,2]

^{1} Department of Materials Science and Engineering, WW4-LKO, University of Erlangen-Nuremberg, Martensstrasse 7, D-91058 Erlangen, Germany

^{2} Chemistry Department, Faculty of Sciences, King Abdulaziz University, 80203 Jeddah, Saudi Arabia Kingdom

*Corresponding author:

Prof. Dr. Patrik Schmuki:

Tel.: +49-9131-852-7575, Fax: +49-9131-852-7582, Email:schmuki@ww.uni-erlangen.de

†These authors equally contributed to this work.

Link to the published article:

In present work, we report on the use of organized TiO_2 nanotube layers with a regular intertube spacing for the growth of highly defined α-Fe_2O_3 nano-needles in the interspace. These α-Fe_2O_3 decorated TiO_2 NTs are then explored for Li-ion battery applications and compared to classic close-packed NTs that are both decorated with various amounts of nanoscale α-Fe_2O_3. We show that nanotubes with tube-to-tube spacing allow a uniform decoration of individual nanotubes with regular arrangements of hematite nano-needles. The tube spacing also facilitates the electrolyte penetration as well as yields better ion diffusion. While bare close-packed NTs show higher capacitance, e.g., 71 μAh cm^{-2} than bare spaced NTs with e.g., 54 μAh cm^{-2}, the hierarchical decoration with secondary metal oxide, α-Fe_2O_3, remarkably enhances the Li-ion battery performance. Namely, spaced nanotubes with α-Fe_2O_3 decoration have an areal capacitance of 477 μAh cm^{-2}, i.e., show up to nearly ~8 times higher capacitance. However, the areal capacitance of close-packed NTs with α-Fe_2O_3 decoration saturates at 208 μAh cm^{-2}, i.e., is limited to ~3 times increase.

Keywords: Anodization, TiO_2 nanotube, Spaced nanotube, Fe_2O_3, Li-ion battery

1. Introduction

Over the last decades, the formation, properties and functionalization of electrochemically formed TiO_2 nanotubes (NTs) attracted considerable interest and such structures have been explored for a broad range of applications, e.g. dye-sensitized solar cells [1,2], photocatalysis [2], biomedicine [3,4] and other energy storage devices [5–7]. Meanwhile, a high level of control over the morphological features of the nanotubes, such as diameter, length, wall thickness, wall morphology, as well as over crystal phases (amorphous, anatase, rutile) has been achieved [5,8]. A range of morphological variations has been produced, including bamboo tubes, branched tubes, the fabrication of membranes, or single-walled TiO_2 NTs [5,9–12].

Generally, self-ordered TiO_2 nanotube arrays grow in a hexagonally close-packed (CP) configuration, i.e., have no or only a minor spacing at the top (top spacing). However, previous research shows that with certain electrolyte compositions, spaced NTs, i.e., showing regular as well as tunable gaps between individual tubes, are obtained [13–16]. This particularly if the organic electrolyte is diethylene glycol (DEG) or dimethyl sulfoxide (DMSO). Few more electrolytes, e.g., ethylene glycol (EG), tri(tetra, poly)-ethylene glycol, were reported to result in the growth of spaced NTs under specific anodization conditions [17,18]. Nanotubes grown on Ti metal, which serves as a back contact, can outperform classic geometries if a conformal/hierarchical decoration is allowed/accommodated [19], as suggested by Simon and Gogotsi for carbon nanotubes [20]. Here, we introduce the use of TiO_2 spaced (SP) nanotubular arrays as a scaffold that offers a wide intertube space to be filled/loaded with a secondary active metal oxide for energy storage application, in the form of Li-ion batteries (LIBs).

Among different electrochemical energy conversion and storage technologies, LIBs provide a high energy density, long cycle life, low self-discharge and are environmentally friendly [5,21,22]. LIBs consist of two Li-intercalation electrodes, a negative electrode (anode, e.g., graphite) and a positive electrode (cathode, e.g., $LiCoO_2$). Graphite is the most common anode material, however, as an anode material it has limitations due to a low specific capacity and poor safety (e.g., dendrite formation) [22–24]. TiO_2 represents an alternative anode material to graphite, since it possesses the combination of sufficient intercalation capacity with a good cyclic stability (low volume expansion, i.e., <4%), low production costs, and low toxicity [25,26].

Various nano-geometries as anode materials for LIB such as nanowires, nanorods, nanoparticles, mesocages, and nanopores/nanotubes have been used [22,27–30]. Nanotubes/nanopores morphologies (by anodization) have an advantage over the other morphologies as they can be directly grown from the metal in a vertically aligned form that

provides electron transport directionality [5,11]. An early attempt of using TiO_2 nanotubes in Li-ion batteries was reported by Zhou et al. in 2003 [25], using hydrothermally grown anatase nanotubes with ~300 nm individual tube length and ~8 nm diameter (specific capacitance, 182 mAh/g at 80 mA/g).

The capacitance of TiO_2 is however limited due to the low electronic conductivity or the high intrinsic resistance [31]. The most widely used techniques to improve the capacitance, are to modify the nanotubes by hierarchical or conformal decoration with highly pseudocapacitive metal oxides, e.g., SnO_2, Co_3O_4, CoO, NiO_2, Fe_2O_3, Nb_2O_5 [5,32–34]. Amongst the various transition metal oxides, Fe_2O_3 is promising owing to its high theoretical capacity (i.e., 1000 mAh g^{-1}), high abundance, and low processing costs [33,35]. Particularly interesting is that the nano-size α-Fe_2O_3 has better electrochemical performance than the micro-size α-Fe_2O_3, as lithium can be inserted in the nanostructure without a phase transformation [33].

In the present work, we grow spaced TiO_2 NTs by electrochemical anodization of a Ti foil in di-ethylene glycol (DEG) electrolyte and then hierarchically coat the tubes with α-Fe_2O_3 nanogeometries. Such TiO_2 nanotubular arrays show a strong improvement of the Li-ion battery performance in comparison to the classic close-packed tube configurations.

2. Experimental section

Prior to anodization, 0.1 mm thick Ti foils (99.6% pure tempered annealed, ADVENT) were degreased by sonication in acetone, ethanol, and distilled water, respectively, and dried under a nitrogen (N_2) stream. To fabricate spaced nanotubes (NTs), anodization was performed in diethylene glycol (DEG) electrolyte with additions of 2 wt% HF (40%), 7 wt% H_2O, and 0.3 wt% NH_4F at 30 V (room temperature) for 10 h. The classic close-packed NTs were formed in 1 M H_2O and 0.1 M NH_4F containing ethylene glycol (EG) electrolyte at an applied voltage of 40 V for 15 min at 50 °C. Anodization was carried out in a two-electrode configuration with Pt as cathode and Ti substrate as anode (IMP-Series Jaissle Potentiostat). After anodization, the samples were immersed in ethanol overnight and dried in a N_2 stream. Before the Fe_2O_3 decoration, the nanotubular layers were annealed at 450 °C (air) for 2 h using a rapid thermal annealer. Iron (III) chloride hexahydrate ($FeCl_3.6H_2O$) was used as a precursor to prepare 10-160 mM suspensions in de-ionized water. β-FeOOH decoration of the nanotubes was carried out by a chemical precipitation technique at 80 °C in an oven (Heraeus, Germany) for 4 h, according to Eq. 1. Subsequently, nanotubes with β-FeOOH decoration were annealed at 400 °C for 2 h in air to form α-Fe_2O_3 [36] according to Eq. 2.

$$Fe^{3+} + 3H_2O \rightarrow FeOOH + 3H^+ \qquad \text{Eq. 1}$$
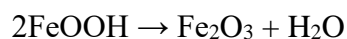
$$2FeOOH \rightarrow Fe_2O_3 + H_2O \qquad\qquad\qquad\qquad Eq. 2$$

2.1 Characterization and measurements

The morphology was characterized using a field-emission SEM (S4800 Hitachi) coupled with an EDX (Genesis 4000). XRD (X'pert PhilipsMPD with a Panalytical X'celerator detector, Germany) was performed using graphite monochromized CuKα radiation (Wavelength 1.54056 Å). The chemical composition was characterized by XPS (PHI 5600, spectrometer, USA) using Al Kα monochromatized radiation (spectra were shifted to C1s a 284.8 eV) and the peaks were fitted with Multipak software.

Electrochemical measurements were conducted in a propylene carbonate electrolyte consisting of 1 M LiClO$_4$ solution at room temperature using a two-electrode setup in Argon filled glove box (MBraun, water and oxygen content below 0.5 ppm). Cyclic voltammetry tests were performed in an electrochemical cell, exposing ≈ 0.567 cm^2 of the sample surface using a two-electrode set-up, i.e. Li metal served as a counter/cathode and the nanotube layer as working electrode/anode. The cyclic voltammetry tests were done in the voltage range of 0–3 V at a scan rate of 1 mV/s (the 5th cycle was considered if not stated otherwise). The galvanostatic charge-discharge tests were conducted using a Swagelok cell that consists of a separator with a working area of ≈ 0.5 cm^2 (i.e., GF/F, Whatman), a Li cathode (Alfa Aesar, Li foil-99.9%), and the tubular layers as an anode.

3. Results and discussion

Figure 1 shows SEM images of spaced and close-packed NTs. The spaced NTs are grown in DEG-based electrolyte at 30 V for 10 h (Figure 1 (a1)–(a2)) under optimized conditions (voltage, temperature, electrolyte composition, e.g., HF, H$_2$O and NH$_4$F) and have a slow growth rate. In general, spaced nanotubes grow under a metastable situation and in the voltage range between 10 to 40 V, while higher or lower voltages than this range lead to porous oxide or only sponge oxide structures, as previously reported [37].

Classic close-packed NTs are used as a reference (CP-TiO$_2$) and fabricated in EG-based electrolyte, see Figure 1 (b1)-(b2). The geometrical features of the as-formed nanotubes are as follows: EG close-packed NTs have a tube diameter of ~81 nm, while DEG spaced NTs have a diameter of ~127 nm, and both spaced and close-packed NTs are ~3 µm long. From the top view, spaced NTs have ring-like features and close-packed NTs have grass-like structures at the top due to over-etching of tube tops in the electrolyte. The significant morphological

difference between close-packed and spaced NTs is that spaced NTs have a spacing (tube-to-tube) of 150±40 nm between the individual NTs.

Another remarkable difference between close-packed and spaced NTs is their wall morphology i.e., double-walled structure (consists of carbon rich inner shell) or single-walled, see Figure 1 (a2)-(b2). In the case of close-packed NTs, a double-walled structure of the nanotubes is revealed from top to bottom. On the other hand, in the case of spaced tubes, the double-walled structure is visible only close to the bottom. Overall, the spacing in between individual nanotubes and the thin-wall structure of spaced NTs will lead to a larger area available for the decoration with secondary oxide materials.
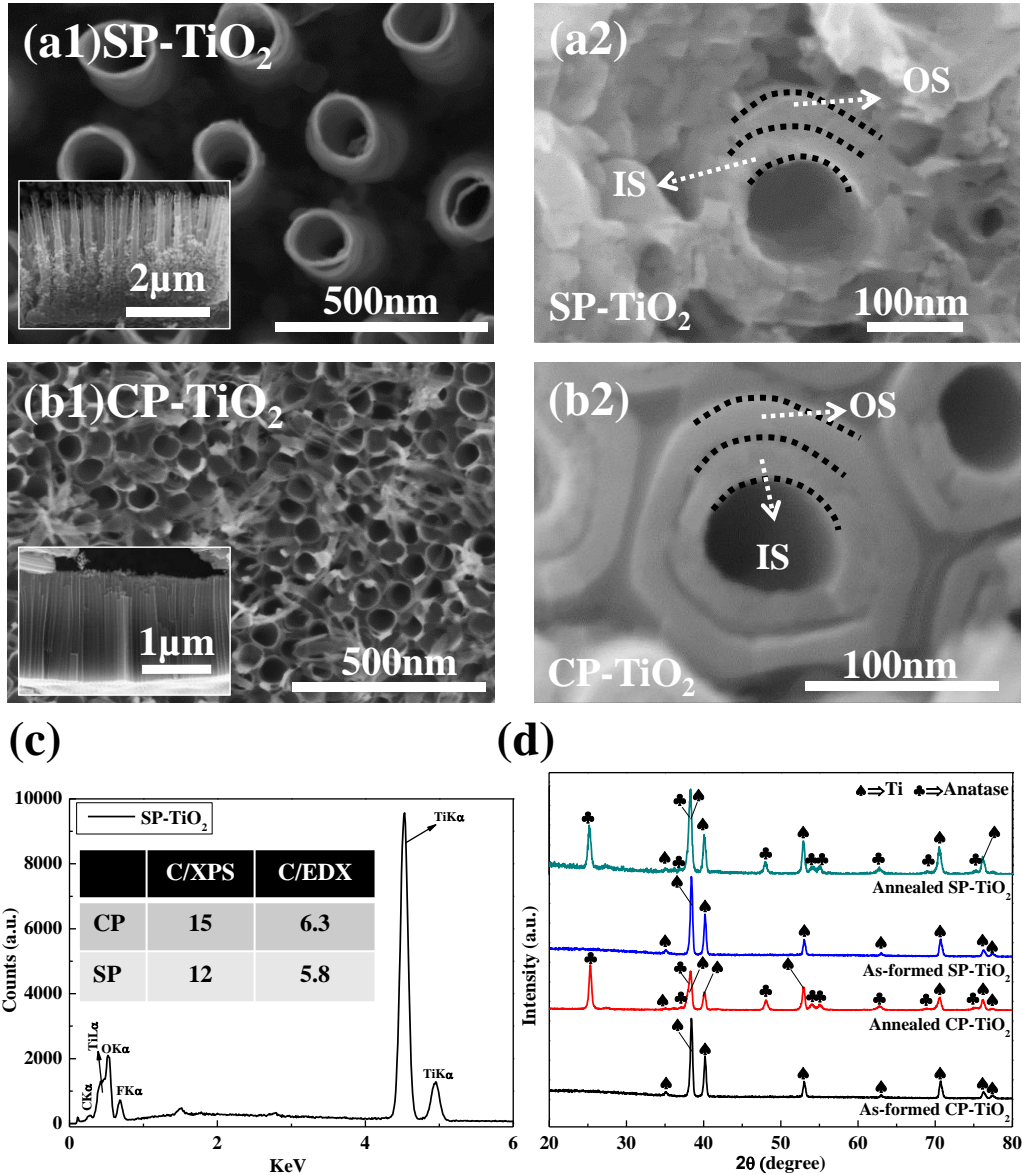

Figure 1 (a1) Top-view and inset cross-section SEM image of spaced TiO_2 nanotubes (SP-TiO_2). **(a2)** Double-wall SP-TiO_2 nanotubes, nanotubes cracked close to the bottom. **(b1)** Top-view and inset cross-section SEM image of close-packed TiO_2 nanotubes (CP-TiO_2). **(b2)**

Double-wall CP-TiO$_2$ nanotubes, nanotubes cracked close to the middle. (**c**) Energy dispersive X-ray spectroscopy (EDX) analysis result for as-formed SP-TiO$_2$ (inset table shows carbon content of as-formed CP-TiO$_2$ and SP-TiO$_2$ measured by XPS and EDX analysis). (**d**) X-ray diffraction (XRD) patterns of as-formed, annealed CP-TiO$_2$ and SP-TiO$_2$ NTs.

Figure 1(c) shows EDX and XPS analysis of spaced and close-packed NTs: both EG and DEG NTs have a higher carbon content at the top most layer. The higher carbon content at the top (in XPS) can be ascribed to the carbon pick-up or adsorption of carbon from the electrolyte. In the case of EDX analysis, CP NTs have a slightly higher carbon content due to carbon rich inner shell from top to bottom.

X-ray diffraction patterns of as-formed and annealed NTs are given in Figure 1(d). After annealing, the anatase-rutile phase composition of structures shows differences as close-packed NTs have an anatase fraction of 92 % (8 % rutile) and spaced NTs have 71 % (29 % rutile). The higher rutile composition of spaced NTs is attributed to the easy conversion of the sponge oxide to rutile. The spongy oxide is concentrated in the lower part of the tubular layer and its amount can increase or decrease depending on the anodization conditions (applied temperature, applied voltage, and water content) [37,38].
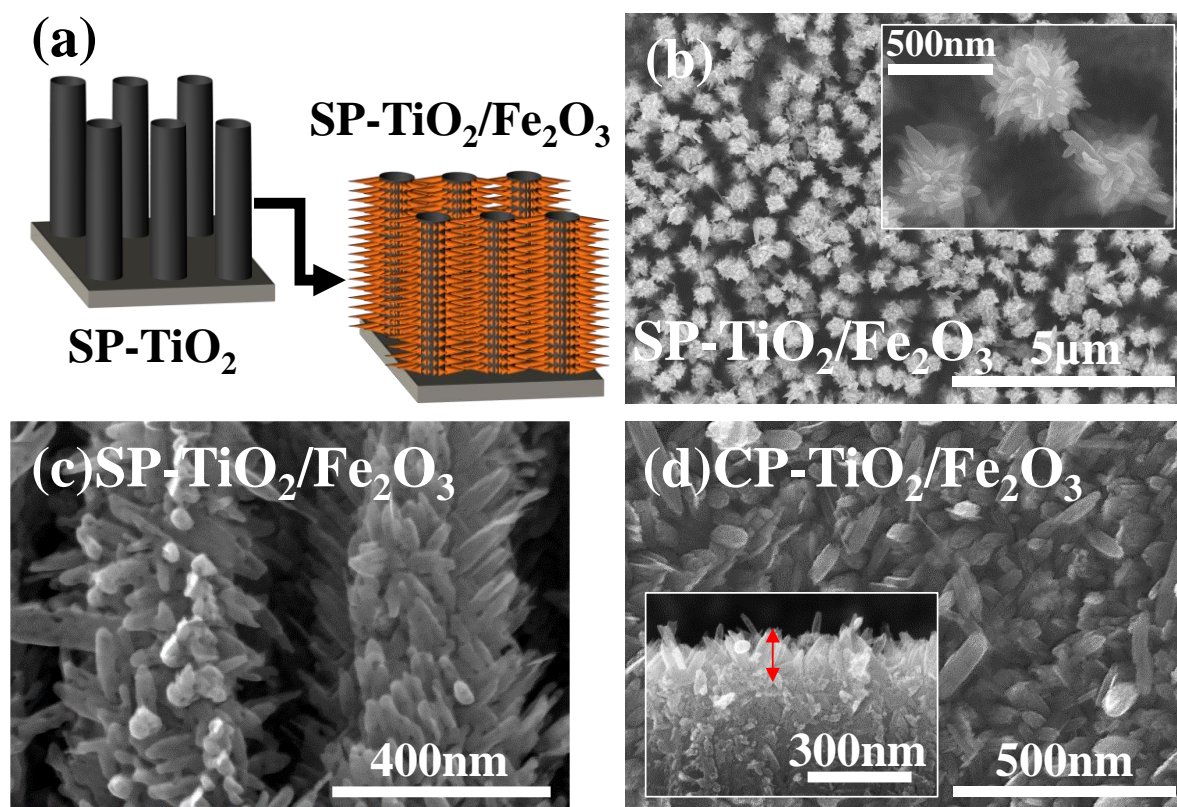

Figure 2 (a) Schematic drawing of bare spaced (SP-TiO$_2$) and Fe$_2$O$_3$ decorated spaced TiO$_2$ NTs (SP-TiO$_2$/Fe$_2$O$_3$). (**b**) Top view (inset shows high magnification image) and (**c**)

cross-section SEM image of Fe_2O_3 decorated spaced TiO_2 nanotubes (SP-TiO_2/Fe_2O_3). **(d)** Top-view and inset cross-section SEM image of Fe_2O_3 decorated close-packed TiO_2 nanotubes (CP-TiO_2/Fe_2O_3).

The assembly of the hierarchical TiO_2/Fe_2O_3 electrode is performed in two-steps: *i)* self-organizing anodization of Ti to form spaced TiO_2 nanotubes (SP-TiO_2), and *ii)* decoration of NTs with α-Fe_2O_3 (SP-TiO_2/Fe_2O_3), as illustrated in Figure 2 and S1-2. α-Fe_2O_3 decoration is established by using $FeCl_3 \cdot 6H_2O$ (in DIW) at 80 °C. The decorated iron is in the form of iron oxyhydroxide and contains Cl^- (see EDX in Figure S3(a)). Afterward the electrode is dried and sintered at 400 °C in air for 2 h to crystallize the iron oxyhydroxide particles according to Eq. 1 and Eq. 2. It is worth mentioning that a similar electrode assembly procedure is followed for close-packed NTs (CP-TiO_2/Fe_2O_3). The obtained α-Fe_2O_3 has a nano-needle structure with sharp tips, see Figure 2(b)–(d), S1-S2. The nano-needles grow on the walls of NTs from top to the bottom and exist regularly between as well as on the inner walls of the NTs, see Figure S4.

To evaluate the optimum α-Fe_2O_3 decoration, both close-packed and spaced nanotubes were decorated in solutions with different Fe-precursor concentrations (i.e., 10 to 160 mM). As expected, spaced NTs can accommodate more α-Fe_2O_3 nano-needles compared with close-packed NTs, i.e., even when the concentration is increased to 160 mM there is no clogging of the tube tops and the α-Fe_2O_3 nano-needles uniformly cover the outer as well as the inner walls of the NTs from tube top to bottom (see Figure 2(b)–(c) for 120 mM, Figure S1 for different loadings from 40 to 160 mM and Figure S5-6 for elemental mapping). Contrary to spaced NTs, in the case of close-packed NTs, low concentrations, for instance 10 mM, lead to open tube tops, however, at high concentrations, such as $\geq$40 mM, α-Fe_2O_3 nano- needles clog the tube openings (see Figure 2(d) and S2).
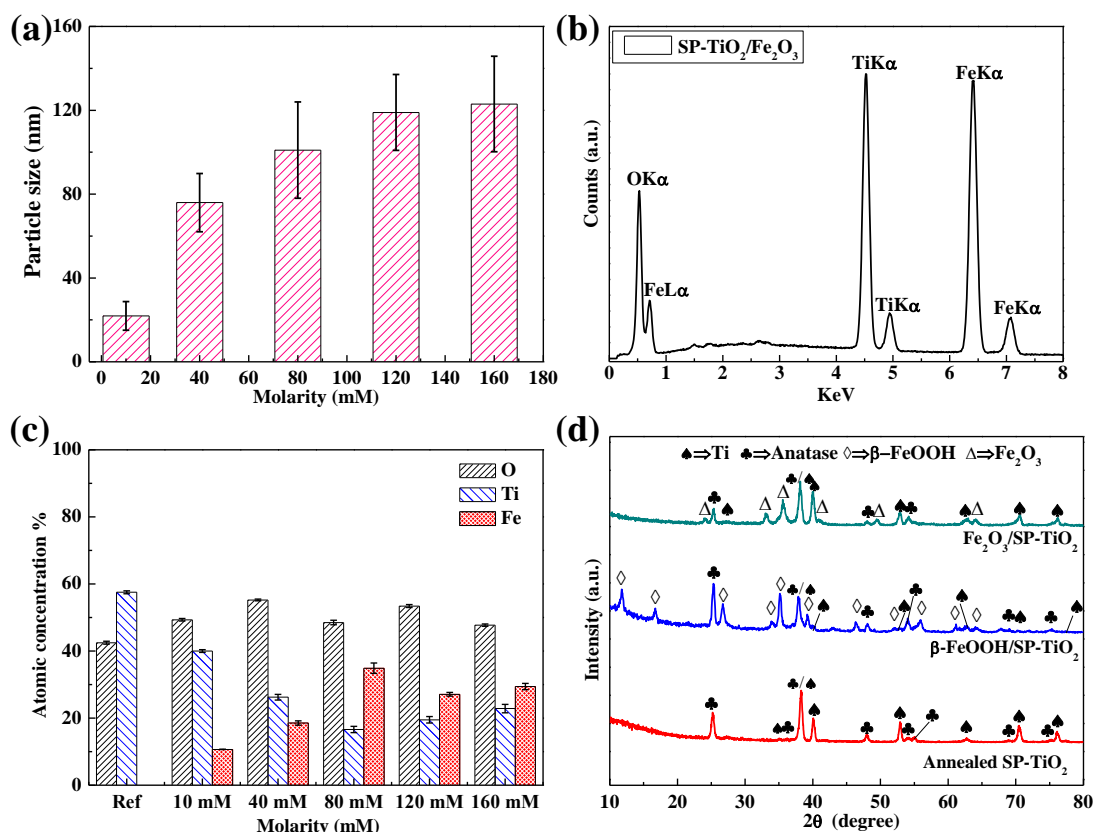
Figure 3 Spaced nanotubes: (a) Variation of the Fe_2O_3 particle size vs. concentration of the iron precursor used for deposition. **(b)** EDX analysis of α-Fe_2O_3 decorated spaced TiO_2 NTs (SP-TiO_2/Fe_2O_3). **(c)** Variation of atomic concentration of Ti, Fe, O as a function of the concentration of iron precursor for bare (SP-TiO_2) and α-Fe_2O_3 decorated spaced NTs (SP-TiO_2/Fe_2O_3) measured by EDX. **(d)** XRD patterns of as-formed, as-deposited β-FeOOH on SP-TiO_2 and α-Fe_2O_3 on SP-TiO_2/ NTs.

The concentration of the iron salt/precursor affects the size of α-Fe_2O_3 nano-needles, i.e., particle size increases with Fe-precursor concentration as shown in Figure 3(a). Literature reports that particle size of iron (III) oxide is controlled by pH, temperature, the nature of the salts, as well as the concentration and furthermore nano-sized iron oxide particles show better performance than micro-sized [33,39,40].

Additionally, the EDX elemental analyses for close-packed and spaced NTs with/without α-Fe_2O_3 decoration obtained using various Fe-precursor concentrations are shown in Figure 3(b)-(c) and S3(b). In the case of close-packed NTs, the atomic ratio of Fe reaches 18.1 for 40–80 mM and then it drastically decreases (Figure S3(b)). On the other hand, for spaced NTs, at 80 mM Fe concentration, the highest Fe content (34.2 at. %) is reached and then it slightly decreases, see Figure 3(c).

9

Figure 3(d) demonstrates X-ray diffraction patterns of spaced nanotubes with/without iron-oxide decoration (see Figure S3(c) for XRD patterns of close-packed NTs with/without α-Fe$_2$O$_3$ decoration). Annealed TiO$_2$ NTs crystallize in the form of anatase (JCPDS 21-1272) and rutile (JCPDS 21-1276). The as-decorated nano-needles are in the form of β-FeOOH (Akaganeite; Tetragonal crystal form) with peaks located at 11.84° (110), 16.79° (200), 26.72° (310), 35° (211), and 55.9° (521). After annealing, the β-FeOOH is converted to hematite, hexagonal crystal form (α-Fe$_2$O$_3$, JCPDS No. 89-0596), with peaks located at 24.13° (012), 33.12° (104), 35.62° (110), 49.4° (024) and 63.97° (300).
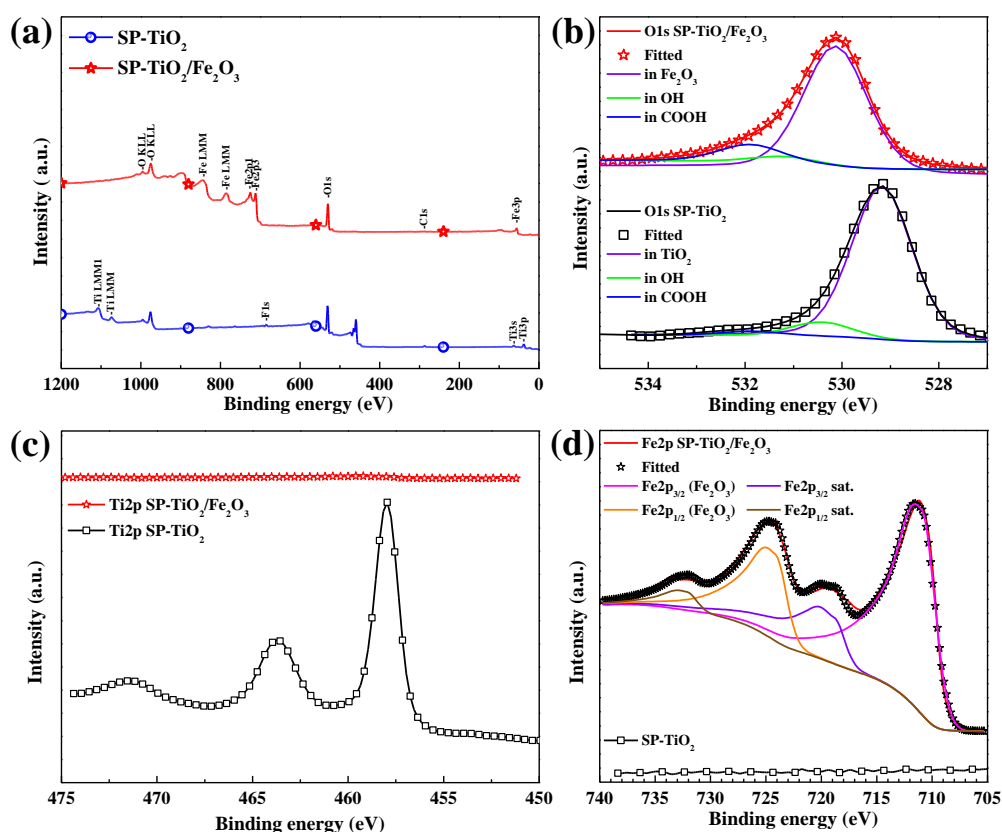
Figure 4 X-ray photoelectron spectroscopy (XPS) analysis: (a) XPS survey spectra of bare SP-TiO$_2$ and α-Fe$_2$O$_3$ decorated spaced (SP-TiO$_2$/Fe$_2$O$_3$) NTs. (**b**) XPS O1s peaks and fittings for SP-TiO$_2$ and SP-TiO$_2$/Fe$_2$O$_3$ nanotubes. (**c**) XPS Ti2p peaks for bare SP-TiO$_2$ and SP-TiO$_2$/Fe$_2$O$_3$ NTs. (**d**) XPS Fe2p peak and fitting for SP-TiO$_2$/Fe$_2$O$_3$ NTs.

The chemical composition of SP-TiO$_2$ and SP-TiO$_2$/Fe$_2$O$_3$ tubular layers was evaluated by XPS as shown in Figure 4. The survey spectra of the as-formed nanotubes confirm the presence of Ti, C, O, F, and after the α-Fe$_2$O$_3$ decoration only Fe, O and C peaks are visible. The high-resolution spectra of O1s (with peak fitting), Ti2p and Fe2p (with peak fitting) are given in Figure 4(b)–(d). The reference sample, that is the bare SP-TiO$_2$ nanotubes, shows the typical

O1s peak consisting of an O signal from TiO_2 at ≈529.2 eV, O from OH bonds at ≈530.4eV and at ≈531.9 eV from C-O, as attributed in Figure 4(b), with the corresponding $Ti2p_{3/2}$ peak at ≈458.0 eV. For the α-Fe_2O_3 decorated samples, no Ti2p signals are observed at the surface, indicating the uniform coverage of TiO_2 tube walls with α-Fe_2O_3. The O1s peak can be associated with the O signal from α-Fe_2O_3 at ≈530.2 eV (in line with literature [41]), O from OH bonds at ≈531.2 eV and at ≈531.9 eV from C-O. As expected, Fe peaks are detected only for the α-Fe_2O_3 decorated samples. The peaks at 710.2 eV ($Fe2p_{3/2}$) and 724.6 eV ($Fe2p_{1/2}$) indicate the presence of α-Fe_2O_3 and are consistent with the values reported in literature for the α-Fe_2O_3 phase [41–43] – this holds for the binding energy values of $Fe2p_{3/2}$ and $Fe2p_{1/2}$ as well as the clearly distinguishable satellite peaks at ≈719.5eV and at ≈732.4eV.

Such hierarchical structures are further evaluated for Li-ion battery (LIB) application and a comparison of the battery performance of the spaced and the close-packed nanotubes is demonstrated in Figure 5. Cyclic voltammetry (CV) and galvanostatic charge/discharge tests were conducted in a propylene carbonate electrolyte consisting of 1 M $LiClO_4$ solution as described in the experimental section. The Li-ion intercalation into TiO_2 lattice occurs according to:

$$xLi^+ + TiO_2 + xe^- \leftrightarrow Li_xTiO_2 \qquad\qquad\qquad \text{Eq. 3}$$

In the CV curves, the Li^+ intercalation peak is observed at 1.64 and 1.61 V for SP-TiO_2 and CP-TiO_2 NTs, and the Li^+ deintercalation peak is located at 2.23 V for SP-TiO_2 and at 2.31 V for CP-TiO_2, respectively. From Figure 5 it is evident that the CV curves of the bare CP-TiO_2 NTs reach a higher current density than the SP-TiO_2 NTs. This is ascribed to the higher surface area (i.e., higher number of nanotubes) for close-packed tubes.
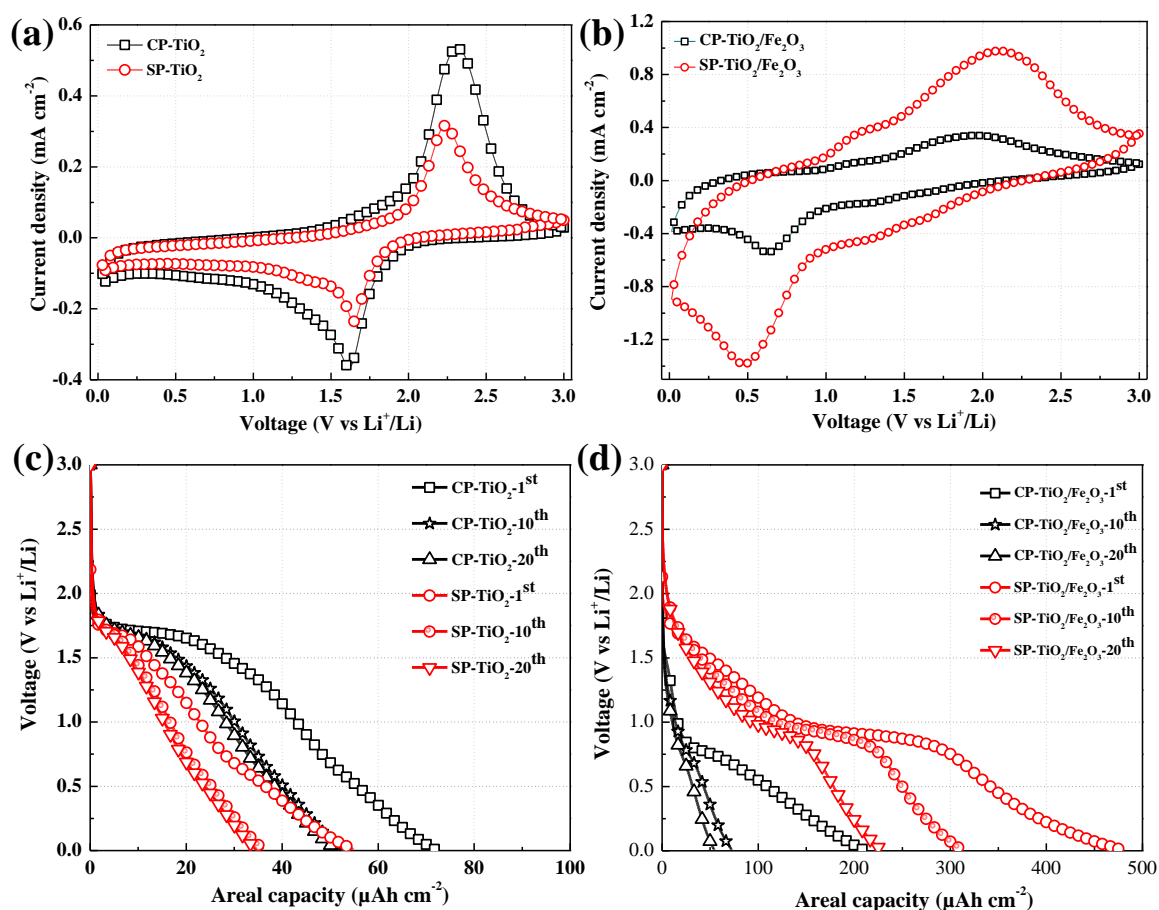
Figure 5 Comparison of battery performance: Cyclic voltammetry (CV) of (**a**) bare spaced (SP-TiO$_2$) and close-packed (CP-TiO$_2$) nanotubes. CV of (**b**) α-Fe$_2$O$_3$ decorated spaced (SP-TiO$_2$/Fe$_2$O$_3$) and close-packed (CP-TiO$_2$/Fe$_2$O$_3$) nanotubes. Comparison of galvanostatic discharge curves of (**c**) SP-TiO$_2$ and CP-TiO$_2$, (**d**) SP-TiO$_2$/Fe$_2$O$_3$ and CP-TiO$_2$/Fe$_2$O$_3$ nanotubes.

The separation between lithiation and delithiation peaks is lower for spaced NTs (i.e., 0.59 V) than close-packed NTs (i.e., 0.69 V), which indicates a faster Li$^+$ diffusion or lower overpotential, as reported previously [44]. In literature, peak to peak separation is reported as 0.45 V for anodic TiO$_2$ nanotubes [45], as 0.36 V for hydrothermal TiO$_2$ nanotubes [46], and as 0.28 V for 10 nm sized TiO$_2$ nanoparticles [44]. The large separation and the deviation from the Nernstian redox reactions (i.e., 59 mV for one electron reaction) are associated with slow electron transport, transport limitations in the electrolyte, a slow reaction kinetics [24,47,48], or can be due to semiconductor nature of TiO$_2$ [49].

We further evaluated the influence of Li$^+$ intercalation as well as deintercalation on the crystal structure of TiO$_2$ as shown in Figure S7. Once the intercalation process takes place, the anatase peak becomes smaller. Upon Li deintercalation a significant reduction in the peak

intensity is observed. The reduction in the peak intensity (due to Li^+ intercalation as well as to deintercalation) can be due to the amorphization of TiO_2, as reported previously [34,50,51].

The influence of secondary metal oxide loading (α-Fe_2O_3) on the LIB performance was investigated for both CP and SP NTs. Figure 5(b) and S8 show the CVs for the close-packed and spaced nanotubular layers decorated with different iron salt concentrations between 10 to 160 mM.

While for spaced NTs the current density increases significantly with increasing concentration (up to 120 mM) of Fe-precursor, in the case of close-packed NTs the current density barely increases and results in a comparable Li-battery performance as for bare close-packed TiO_2 NTs (see Figure S8). The findings for spaced nanotubes suggest that 120 mM provides an optimal loading with the current density reaching the peak point. This means that for the SP NTs, although they have less surface area than the CP tubes, the spacing enables an easy access for the deposition of a secondary metal oxide. Additionally, the spacing between NTs promotes electrolyte penetration during Li^+ insertion/extraction. The cathodic peak at about 0.47 V indicates a complete reduction of Fe^{+3} to Fe^0 and the formation of Li_2O. The wide cathodic peak may be an indication of the formation of an irreversible solid-electrolyte interphase (SEI) formation. In the anodic polarization/sweep process (i.e., delithiation), a wide peak (composed of two peaks) was recorded at about 2.1 V corresponding to the oxidation of Fe^0 to Fe^{+3} and delithiation of TiO_2, respectively (Figure 5(b)), as described in literature [52].

Figure 5(c)–(d) illustrate the galvanostatic discharge curves for bare and α-Fe_2O_3 decorated nanotubes. In the galvanostatic discharge cycle of bare close-packed and spaced NTs, the potential rapidly drops to reach a well-defined plateau at 1.75 V associated with the intercalation of Li^+ through a two-phase equilibrium of a Li-poor (tetragonal) and a Li-rich (orthorhombic) phase, see Figure 5(c). In previous works, a Li intercalation plateau is observed at ~1.7 V and at ~1.8 V for anodic TiO_2 NTs [53,54], at ~1.76 V for hydrothermally grown TiO_2 NTs [46] and at 1.8 V for anatase TiO_2 nanoparticles [55]. In the case of iron decorated nanotubes, a broad band between 1.5 and 0.7 V with a maximum at ~1 V is visible, meaning that Fe^{3+} ions are reduced to Fe^0 (Figure 5d), in line with literature [50].

The voltage (vs. Li/Li^+) versus areal capacity graph shows that the capacity calculated from the 1st discharge cycle for close-packed and spaced bare NTs are 71 µAh cm^{-2} (~51 µAh cm^{-2} for 20th discharge cycle), 54 µAh cm^{-2} (~34 µAh cm^{-2} for 20th discharge cycle) at the rate of 0.2 mA cm^{-2}, respectively (Figure 5(c)). The reported capacitance values for TiO_2 vary depending on the morphology, crystal structure and further treatments. Wei et al. [56] produced 4.5, 9 and 14.5 µm long smooth NTs using two-step anodization. These 9 µm smooth NTs provide high

and stable areal capacities of 0.24 mAh/cm^2 at a charge/discharge current density of 2.5 mA/cm^2. For longer nanotubes e.g. 14.5 µm, an areal capacity of 0.70 mAh/cm^2 was obtained in the first cycles, which decreased to 0.60 mAh/cm^2 after 100 cycles.

The α-Fe$_2$O$_3$ loaded spaced TiO$_2$ nanotubes show an areal capacitance of 477 µAh cm^{-2} – that is an approximately ~8 times increase compared with close-packed NTs (208 µAh cm^{-2}, limited to ~3 times increase, note that 1st cycles are considered for comparison), see Figure 5(d). The increase in capacitance is attributed to the fact that spaced NTs not only lead to good amount of metal oxide loading but also promote electrolyte penetration and better use of the active surface area for Li-ion intercalation.

Here, we observe a comparable performance for α-Fe$_2$O$_3$ loaded TiO$_2$ nanotubes with previously published results. For instance, Ortiz et al. [50,57] demonstrated titania nanotube and iron oxide nanowire composites negative electrode that is built by combining an anodic TiO$_2$ layer with electrodeposited Fe$_2$O$_3$ nanowires. The 3 µm thick nanocomposite electrode exhibited areal capacities of 468 mAh/cm^2 (specific capacities of 1190 mAh/g) at a rate of 25 mA/cm^2. Yu et al. [36] reported 600 µAh/cm^2 at a current density of 50 mA/cm^2 for 10 µm TiO$_2$ NTs decorated with Fe$_2$O$_3$ nanoparticles.

The bare spaced and close-packed NTs show good cyclic stability, i.e. close-packed NTs retain 84% and spaced NTs 53% of their initial capacities for a higher number of cycles. On the other hand, Fe$_2$O$_3$ decorated TiO$_2$ NTs show poorer cyclic stability due to Fe$_2$O$_3$ dominated electrochemical response of Fe$_2$O$_3$/TiO$_2$ electrodes. The poor cyclic performance of Fe$_2$O$_3$/TiO$_2$ electrodes is attributed to low electrical conductivity and iron oxide aggregation during charging/discharging, while TiO$_2$ NTs still maintain their morphology i.e., present no crack/fracture formation and show morphological stability.

4. Conclusion

The present study demonstrates the possibility to decorate the inner and outer walls of spaced TiO$_2$ nanotubular arrays (i.e. nanotubes with tube to tube spacing) with α-Fe$_2$O$_3$ nano-needles, and thus enhance their functional features. For this, the loading of spaced and close-packed nanotubes at different Fe-precursor concentrations are evaluated and optimum loading is achieved.

Overall, a spaced nanotubular TiO$_2$ array with optimum α-Fe$_2$O$_3$ (SP-TiO$_2$/Fe$_2$O$_3$) loading leads to improved Li-ion battery performance. I.e., the bare spaced NTs provide a 54 µAs cm^{-2} capacitance, the functionalized electrodes (SP-TiO$_2$/Fe$_2$O$_3$), decorated with an optimized loading yield an areal capacitance of 477 µAh cm^{-2}. On the other hand, classic close-packed

NTs with α-Fe$_2$O$_3$ decoration (CP-TiO$_2$/Fe$_2$O$_3$) show an areal capacitance of 208 µAh cm^{-2} – this value is restricted by the limited loading volume of this geometry. Furthermore, we believe that this concept, to load spaced tubular configuration with a secondary active or synergistic material not only is beneficial for an improved Li-ion battery performance of TiO$_2$ structures but also can find wider applications in further functional hierarchical structures.

Acknowledgements

References

[1]   Zhu K, Vinzant T B, Neale N R and Frank A J 2007 Removing structural disorder from oriented TiO_2 nanotube arrays: Reducing the dimensionality of transport and recombination in dye-sensitized solar cells *Nano Letters* **7** 3739–46

[2]   Zhu K, Neale N R, Miedaner A and Frank A J 2007 Enhanced charge-collection efficiencies and light scattering in dye-sensitized solar cells using oriented TiO_2 nanotubes arrays *Nano Letters* **7** 69–74

[3]   Park J, Bauer S, von der Mark K and Schmuki P 2007 Nanosize and vitality: TiO_2 nanotube diameter directs cell fate *Nano Letters* **7** 1686–91

[4]   Popat K C, Leoni L, Grimes C A and Desai T A 2007 Influence of engineered titania nanotubular surfaces on bone cells *Biomaterials* **28** 3188–97

[5]   Lee K, Mazare A and Schmuki P 2014 One-dimensional titanium dioxide nanomaterials: nanotubes *Chemical Reviews* **114** 9385–454

[6]   Fang D, Huang K, Liu S and Li Z 2008 Electrochemical properties of ordered TiO_2 nanotube loaded with Ag nano-particles for lithium anode material *Journal of Alloys and Compounds* **464** L5–9

[7]   Liu D, Zhang Y, Xiao P, Garcia B B, Zhang Q, Zhou X, Jeong Y-H and Cao G 2009 TiO_2 nanotube arrays annealed in CO exhibiting high performance for lithium ion intercalation *Electrochimica Acta* **54** 6816–20

[8]   Roy P, Berger S and Schmuki P 2011 TiO_2 nanotubes: Synthesis and applications *Angewandte Chemie - International Edition* **50** 2904–39

[9]   Kim D, Ghicov A, Albu S P and Schmuki P 2008 Bamboo-type TiO_2 nanotubes: Improved conversion efficiency in dye-sensitized solar cells *Journal of the American Chemical Society* **130** 16454–5

[10]   Das C, Roy P, Yang M, Jha H and Schmuki P 2011 Nb doped TiO_2 nanotubes for enhanced photoelectrochemical water-splitting *Nanoscale* **3** 3094–6

[11]   Riboni F, Nguyen N T, So S and Schmuki P 2016 Aligned metal oxide nanotube arrays: key-aspects of anodic TiO_2 nanotube formation and properties *Nanoscale Horizons* **1** 445–66

[12]   Hwang I, So S, Mokhtar M, Alshehri A, Al-Thabaiti S A, Mazare A and Schmuki P 2015 Single-walled TiO_2 nanotubes: Enhanced carrier-transport properties by $TiCl_4$ treatment *Chemistry - A European Journal* **21** 9204–8

[13]   Ruan C, Paulose M, Varghese O K, Mor G K and Grimes C A 2005 Fabrication of highly ordered TiO_2 nanotube arrays using an organic electrolyte *The journal of*

physical chemistry. B **109** 15754–9

[14]   Albu S P and Schmuki P 2010 TiO$_2$ nanotubes grown in different organic electrolytes: Two-size self-organization, single vs. double-walled tubes, and giant diameters *physica status solidi (RRL) - Rapid Research Letters* **4** 215–7

[15]   Yoriya S, Mor G K, Sharma S and Grimes C A 2008 Synthesis of ordered arrays of discrete, partially crystalline titania nanotubes by Ti anodization using diethylene glycol electrolytes *Journal of Materials Chemistry* **18** 3332–6

[16]   Yoriya S 2012 Effect of inter-electrode spacing on electrolyte properties and morphologies of anodic TiO$_2$ nanotube array films *International Journal of Electrochemical Science* **7** 9454–64

[17]   Chen Y, Lu H, Wang X and Lu S 2012 Large-scale sparse TiO$_2$ nanotube arrays by anodization *Journal of Materials Chemistry* **22** 5921

[18]   Allam N K and Grimes C A 2009 Room temperature one-step polyol synthesis of anatase TiO$_2$ nanotube arrays: Photoelectrochemical properties *Langmuir* **25** 7234–40

[19]   Ozkan S, Nguyen N T, Hwang I, Mazare A and Schmuki P 2017 Highly conducting spaced TiO$_2$ nanotubes enable defined conformal coating with nanocrystalline Nb$_2$O$_5$ and high performance supercapacitor applications *Small* **13** 1603821

[20]   Simon P and Gogotsi Y 2008 Materials for electrochemical capacitors *Nature Materials* **7** 845–54

[21]   Salari M, Aboutalebi S H, Konstantinov K and Liu H K 2011 A highly ordered titania nanotube array as a supercapacitor electrode *Physical Chemistry Chemical Physics* **13** 5038

[22]   Bruce P G, Scrosati B and Tarascon J-M 2008 Nanomaterials for rechargeable lithium batteries *Angewandte Chemie International Edition* **47** 2930–46

[23]   Lukatskaya M R, Dunn B and Gogotsi Y 2016 Multidimensional materials and device architectures for future hybrid energy storage *Nature Communications* **7** 12647

[24]   van de Krol R, Goossens A and Schoonman J 1999 Spatial extent of lithium intercalation in anatase TiO$_2$ *The Journal of Physical Chemistry B* **103** 7151–9

[25]   Zhou Y, Cao L, Zhang F, He B and Li H 2003 Lithium insertion into TiO$_2$ nanotube prepared by the hydrothermal process *Journal of The Electrochemical Society* **150** A1246

[26]   Kirchgeorg R, Kallert M, Liu N, Hahn R, Killian M S and Schmuki P 2016 Key factors for an improved lithium ion storage capacity of anodic TiO$_2$ nanotubes *Electrochimica Acta* **198** 56–65

17

[27]   Byeon A, Boota M, Beidaghi M, Aken K V, Lee J W and Gogotsi Y 2015 Effect of hydrogenation on performance of $TiO_2(B)$ nanowire for lithium ion capacitors *Electrochemistry Communications* **60** 199–203

[28]   Liu C, Gillette E I, Chen X, Pearse A J, Kozen A C, Schroeder M A, Gregorczyk K E, Lee S B and Rubloff G W 2014 An all-in-one nanopore battery array *Nature Nanotechnology* **9** 1031–9

[29]   Xiong Q, Tu J, Xia X, Zhao X, Gu C and Wang X 2013 A three-dimensional hierarchical Fe_2O_3@NiO core/shell nanorod array on carbon cloth: a new class of anode for high-performance lithium-ion batteries *Nanoscale* **5** 7906

[30]   Hong Z, Zhou K, Huang Z and Wei M 2015 Iso-oriented anatase TiO_2 mesocages as a high performance anode material for sodium-ion storage *Scientific Reports* **5** 11960

[31]   Stiller M, Barzola-Quiquia J, Lorite I, Esquinazi P, Kirchgeorg R, Albu S P and Schmuki P 2013 Transport properties of single TiO_2 nanotubes *Applied Physics Letters* **103** 173108

[32]   Augustyn V, Come J, Lowe M A, Kim J W, Taberna P-L, Tolbert S H, Abruña H D, Simon P and Dunn B 2013 High-rate electrochemical energy storage through Li^+ intercalation pseudocapacitance *Nature Materials* **12** 518–22

[33]   Larcher D, Masquelier C, Bonnin D, Chabre Y, Masson V, Leriche J-B and Tarascon J-M 2003 Effect of particle size on lithium intercalation into α-Fe_2O_3 *Journal of The Electrochemical Society* **150** A133-139

[34]   Poizot P, Laruelle S, Grugeon S, Dupont L and Tarascon J-M 2000 Nano-sized transition-metal oxides as negative-electrode materials for lithium-ion batteries *Nature* **407** 496–9

[35]   Sarradin J, Guessous A and Ribes M 1996 Synthesis and characterization of lithium intercalation electrodes based on iron oxide thin films *Journal of Power Sources* **62** 149–54

[36]   Yu L, Wang Z, Zhang L, Wu H Bin and Lou X W (David) 2013 TiO_2 nanotube arrays grafted with Fe_2O_3 hollow nanorods as integrated electrodes for lithium-ion batteries *J. Mater. Chem. A* **1** 122–7

[37]   Ozkan S, Nguyen N T, Mazare A, Hahn R, Cerri I and Schmuki P 2017 Fast growth of TiO_2 nanotube arrays with controlled tube spacing based on a self-ordering process at two different scales *Electrochemistry Communications* **77** 98–102

[38]   Ozkan S, Nguyen N T, Mazare A, Cerri I and Schmuki P 2016 Controlled spacing of self-organized anodic TiO_2 nanotubes *Electrochemistry Communications* **69** 76–9

[39]   Mohapatra M and Anand S 2011 Synthesis and applications of nano-structured iron oxides/hydroxides – a review *International Journal of Engineering, Science and Technology* **2** 127–46

[40]   Chen M, Zhao E, Yan Q, Hu Z, Xiao X and Chen D 2016 The effect of crystal face of Fe_2O_3 on the electrochemical performance for lithium-ion batteries *Scientific Reports* **6** 29381

[41]   Grosvenor A P, Kobe B A, Biesinger M C and McIntyre N S 2004 Investigation of multiplet splitting of Fe 2p XPS spectra and bonding in iron compounds *Surface and Interface Analysis* **36** 1564–74

[42]   Yamashita T and Hayes P 2008 Analysis of XPS spectra of Fe^{2+} and Fe^{3+} ions in oxide materials *Applied Surface Science* **254** 2441–9

[43]   Liu J, Yang S, Wu W, Tian Q, Cui S, Dai Z, Ren F, Xiao X and Jiang C 2015 3D flowerlike α-Fe_2O_3@TiO_2 core-shell nanostructures: General synthesis and enhanced photocatalytic performance *ACS Sustainable Chemistry and Engineering* **3** 2975–84

[44]   Wang J, Polleux J, Lim J and Dunn B 2007 Pseudocapacitive contributions to electrochemical energy storage in TiO_2 (anatase) nanoparticles *The Journal of Physical Chemistry C* **111** 14925–31

[45]   Smith K A, Savva A I, Deng C, Wharry J P, Hwang S, Su D, Wang Y, Gong J, Xu T, Butt D P and Xiong H 2017 Effects of proton irradiation on structural and electrochemical charge storage properties of TiO_2 nanotube electrodes for lithium-ion batteries *Journal of Materials Chemistry A* **5** 11815–24

[46]   He B-L, Dong B and Li H-L 2007 Preparation and electrochemical properties of Ag-modified TiO_2 nanotube anode material for lithium–ion battery *Electrochemistry Communications* **9** 425–30

[47]   Lindström H, Södergren S, Solbrand A, Rensmo H, Hjelm J, Hagfeldt A and Lindquist S-E 1997 Li^+ ion insertion in TiO_2 (anatase). 2. Voltammetry on nanoporous films *The Journal of Physical Chemistry B* **101** 7717–22

[48]   Madian M, Giebeler L, Klose M, Jaumann T, Uhlemann M, Gebert A, Oswald S, Ismail N, Eychmüller A and Eckert J 2015 Self-organized TiO_2/CoO nanotubes as potential anode materials for lithium ion batteries *ACS Sustainable Chemistry & Engineering* **3** 909–19

[49]   Zhang G, Huang C, Zhou L, Ye L, Li W and Huang H 2011 Enhanced charge storage by the electrocatalytic effect of anodic TiO_2 nanotubes *Nanoscale* **3** 4174–81

[50]   Ortiz G F, Hanzu I, Lavela P, Tirado J L, Knauth P and Djenizian T 2010 A novel

architectured negative electrode based on titania nanotube and iron oxide nanowire composites for Li-ion microbatteries *Journal of Materials Chemistry* **20** 4041–6

[51]   Gnanavel M, Pralong V, Lebedev O I, Caignaert V, Bazin P and Raveau B 2014 Lithium intercalation into the jarosite-type hydroxysulfate: A topotactic reversible reaction from a crystalline phase to an inorganic polymer-like structure *Chemistry of Materials* **26** 4521–7

[52]   Chen J, Xu L, Li W and Gou X 2005 α-Fe_2O_3 nanotubes in gas sensor and lithium-ion battery applications *Advanced Materials* **17** 582–6

[53]   Fang H-T, Liu M, Wang D-W, Sun T, Guan D-S, Li F, Zhou J, Sham T-K and Cheng H-M 2009 Comparison of the rate capability of nanostructured amorphous and anatase TiO_2 for lithium insertion using anodic TiO_2 nanotube arrays *Nanotechnology* **20** 225701

[54]   Wu Q L, Li J, Deshpande R D, Subramanian N, Rankin S E, Yang F and Cheng Y-T 2012 Aligned TiO_2 nanotube arrays as durable lithium-ion battery negative electrodes *The Journal of Physical Chemistry C* **116** 18669–77

[55]   Wang D, Choi D, Li J, Yang Z, Nie Z, Kou R, Hu D, Wang C, Saraf L V, Zhang J, Aksay I a and Liu J 2009 Self-assembled TiO_2–graphene hybrid nanostructures for enhanced Li-ion insertion *ACS Nano* **3** 907–14

[56]   Wei W, Oltean G, Tai C-W, Edström K, Björefors F and Nyholm L 2013 High energy and power density TiO_2 nanotube electrodes for 3D Li-ion microbatteries *Journal of Materials Chemistry A* **1** 8160–9

[57]   Ortiz G F, Hanzu I, Djenizian T, Lavela P, Tirado J L, Knauth P and Tirado L 2009 Alternative Li-ion battery electrode based on self-organized titania nanotubes *Chemistry of Materials* **21** 63–7